Small-Angle X-Ray Scattering Reveals the Solution Structure of the Full-Length DNA Gyrase A Subunit

Lionel Costenaro,[1] J. Günter Grossmann,[2]
Christine Ebel,[3] and Anthony Maxwell[1,*]
[1]Department of Biological Chemistry
John Innes Centre
Norwich Research Park
Colney, Norwich NR4 7UH
United Kingdom
[2]Molecular Biophysics Group
CCLRC Daresbury Laboratory
Daresbury, Warrington WA4 4AD
United Kingdom
[3]Laboratoire de Biophysique Moléculaire
Institut de Biologie Structurale
(UMR 5075 CEA-CNRS-UJF)
41 Rue Jules Horowitz
38027, Grenoble
France

Summary

DNA gyrase is the topoisomerase uniquely able to actively introduce negative supercoils into DNA. Vital in all bacteria, but absent in humans, this enzyme is a successful target for antibacterial drugs. From biophysical experiments in solution, we report the low-resolution structure of the full-length A subunit (GyrA). Analytical ultracentrifugation shows that GyrA is dimeric, but nonglobular. Ab initio modeling from small-angle X-ray scattering allows us to retrieve the molecular envelope of GyrA and thereby the organization of its domains. The available crystallographic structure of the amino-terminal domain (GyrA59) forms a dimeric core, and two additional pear-shaped densities closely flank it in an unexpected position. Each accommodates very well a carboxyl-terminal domain (GyrA-CTD) built from a homologous crystallographic structure. The uniqueness of gyrase is due to the ability of the GyrA-CTDs to wrap DNA. Their position within the GyrA structure strongly suggests a large conformation change of the enzyme upon DNA binding.

Introduction

Topoisomerases catalyze the interconversion between different topological forms of DNA in all cells. They play a major role in crucial cellular processes such as transcription, recombination, and replication (Champoux, 2001; Wang, 2002). These enzymes can relax, or introduce positive or negative supercoils into closed domains of DNA. They can also catenate or decatenate closed-circular DNAs, and remove or introduce knots into DNA rings. Topoisomerases transiently cleave a segment of DNA, the gate (or "G") segment, by a transesterification between a tyrosine of the enzyme and a DNA phosphate group. Another DNA segment ("T") is then transported through this break before its religa-

*Correspondence: tony.maxwell@bbsrc.ac.uk

tion. The type I topoisomerases are monomeric and cleave a single strand of the DNA, whereas the type II topoisomerases are dimeric and cleave both strands and transport a second DNA duplex, generally triggered by ATP binding. Because of their vital roles in cells, topoisomerases have become important targets of anticancer chemotherapeutics and antibacterial drugs (Emmerson and Jones, 2003; Hande, 1998; Maxwell and Lawson, 2003; Pommier et al., 1998), some of which are currently in widespread clinical use. Many of the most successful drugs trap the enzyme in a covalent complex with the DNA, leading to cell death.

DNA gyrase, a type II topoisomerase, is an effective target of quinolone antibacterial drugs, such as ciprofloxacin, for two main reasons. First, gyrase is essential in all bacteria and has not been found in humans or more generally in eukaryotes, except recently in plant organelles (Wall et al., 2004). Second, gyrase is the only topoisomerase able to actively introduce negative supercoils into DNA. However, increasing drug resistance is now a serious problem and new agents are urgently needed (Drlica and Malik, 2003). A complete structural and mechanistic understanding of DNA gyrase would greatly assist rational drug-design programs.

DNA gyrase from *Escherichia coli* consists of two subunits, GyrA (97 kDa) and GyrB (90 kDa), the active enzyme being a heterotetramer A_2B_2. GyrB consists of two domains: an amino-terminal domain (NTD) of 43 kDa and a carboxyl-terminal domain (CTD) of 47 kDa. GyrB-NTD has an ATPase activity and dimerizes upon ATP binding, like a clamp. Its X-ray crystallographic structures were solved in complex with a nonhydrolyzable ATP analog, and with the coumarin drug novobiocin bound to a shorter 24 kDa fragment (Lewis et al., 1996; Wigley et al., 1991). GyrB-CTD interacts with the A subunit and plays a role in DNA binding. There is currently no structure of GyrB-CTD; however, X-ray crystallographic structures are known for a homologous domain within yeast topoisomerase II (Berger et al., 1996; Fass et al., 1999). GyrA also consists of two domains: an amino-terminal domain of 59 kDa (GyrA59) and a carboxyl-terminal domain of 38 kDa (GyrA-CTD). GyrA59 contains the active-site tyrosine (Tyr[122]) residues responsible for the cleavage and religation activity of gyrase. Its X-ray crystallographic structure shows a heart-shaped arrangement with two dimer interfaces (see blue domain in Figure 4) (Morais Cabral et al., 1997). The amino-terminal interface forms a positively charged saddle-like surface with the two active-site tyrosines lying near the center. It is thought to be the binding region for duplex DNA (the G segment) and to form the DNA gate. A cavity between the two interfaces is large enough to accommodate the T segment that could be released through opening of the carboxyl-terminal, or "exit" gate. The second domain of GyrA, GyrA-CTD, is inactive on its own, but it binds and wraps DNA around itself (Corbett et al., 2004; Reece and Maxwell, 1991). When it is part of the full-length GyrA, GyrA-CTD is responsible for the unique capacity of gyrase to introduce negative supercoils (Kampranis

and Maxwell, 1996). GyrA-CTD should present the T segment over the G segment, forming a positive cross-over that will be inverted upon the passage of the T segment through the open DNA gate, creating two negative supercoils (see Figure 8) (Brown and Cozza-relli, 1979; Heddle et al., 2004). GyrA-CTD was predicted to adopt a β propeller fold (Qi et al., 2002). Recently, the X-ray crystallographic structure of its homologous domain from *Borrelia burgdorferi* was solved: it is a 6-bladed "β pinwheel," a new fold globally reminiscent of a β propeller with a new blade topology (Corbett et al., 2004). Structural information on the full-length GyrA and understanding the specific mechanism of DNA gyr-ase could reveal new possibilities for drug targeting. There is currently no structural information on full-length gyrase subunits or for any other DNA topoisom-erase.

Here we present the low-resolution structure of full-length GyrA. Sedimentation velocity experiments es-tablish the dimeric state of GyrA in solution. Ab initio modeling allows us to retrieve the global structure of GyrA from small-angle X-ray scattering (SAXS) experi-ments in solution. It reveals a distinctive molecular en-velope for GyrA-CTD, which accommodates very well its high-resolution model built from a homologous crys-tallographic structure. The unexpected position of the CTDs within GyrA provides an important clue toward the understanding of the holoenzyme mechanism and how it is distinct from that of other topoisomerases.

Results

Analytical Ultracentrifugation

Velocity experiments revealed that, in solution, GyrA is a dimer. The sedimentation profiles were directly mod-eled in terms of a continuous distribution of discrete and noninteracting species. A typical set of experimen-tal profiles and modeling is shown in Figure 1A, for the interference data at a protein concentration of 0.9 mg/ml. The corresponding sedimentation-coefficient distri-bution $c(s)$ is represented in Figure 1B with the results obtained at 0.3 and 3.6 mg/ml. GyrA was found to sedi-ment essentially as a single species: the main peaks in $c(s)$ accounted for 96% of the total cell contents and 86% for the lowest protein concentration. Its sedi-mentation coefficient (s) varied between 4.95 and 5.28 S, slightly increasing when the protein concentra-tion decreased. The s value extrapolated at zero protein concentration was 5.25 ± 0.1 S at 6°C, giving an $s°_{20,w}$ of 8 S when normalized to water at 20°C. Assuming a partial specific volume of 0.74 ml/g, this sedimentation coefficient corresponds to a 194 kDa dimer with a hy-drodynamic radius (R_H) of 55.7 ± 1 Å. As the minimal R_H value is 38 Å for the filled sphere with the same mass and density, and 43 Å for the hydrated sphere (0.3 g of water per gram of protein), it implies that GyrA is not globular, but elongated or has cavities.

Small-Angle X-Ray Scattering

The intensity scattered by GyrA in solution was col-lected over the momentum transfer range $0.008 < q < 0.78$ Å^{-1}, corresponding to a real distance range of $762 > r > 8$ Å (Figure 2). The radius of gyration (R_g) of GyrA, calculated from the Guinier approximation, was 54.8 ± 1.5 Å. Its estimation from the second moment of the pair distribution function $p(r)$ led to a consistent value of 53.3 ± 0.5 Å. A sphere with the GyrA mass and density would have an R_g of 30 Å, again showing GyrA to be an extended molecule. The $p(r)$ function (Figure 2, inset), which is the distribution histogram of interatomic distances within the molecule, confirmed this: it had an asymmetric bell shape with a tail extending to a maxi-mum protein dimension (D_{max}) of 167 ± 5 Å.

Ab Initio Modeling

Low-resolution models were generated by two ab initio programs Gasbor and Credo (Petoukhov et al., 2002; Svergun et al., 2001). Both programs represent the pro-tein by clustered spherical dummy residues and use simulated annealing to build a locally "chain-compati-ble" model, with a 3.8 Å separation between dummy residues, inside a spherical search volume. The result is a three-dimensional arrangement of scattering centers that reproduce the one-dimensional scattering curve in accord with the experimental data (Figure 2). As this inverse scattering problem has no unique solution, sev-eral independent models are built and compared to an-alyze the convergence of the structures.

We first attempted to retrieve the global structure of GyrA from SAXS in solution with Gasbor. All dummy residues were refined and a 2-fold symmetry was con-strained as implied by the analytical ultracentrifugation results. Twenty independent runs did not converge to-ward a unique solution, nor toward several subpopul-ations, but rather gave a range of shapes (Figures 3A–3C). The normalized spatial discrepancy (NSD) ranged from 1.6 to 2.7 after realignment of the models. NSD provides a quantitative estimate of the similarity be-tween two models: a lower value corresponds to a bet-ter overlap and a value of around one indicates a good agreement. However, the average model (Figure 3D), representing the common structural features of all the reconstructions, was an oblate ellipsoid large enough to accommodate the GyrA59 structure in its middle with additional density on both sides. The average model also showed a small hole in its center, reminis-cent of the GyrA59 cavity.

Because of these common features, we recon-structed the GyrA solution structure with Credo that al-lowed fixing the GyrA59 residues to their C_α crystallo-graphic position and to refine only the GyrA-CTD residue positions, still constraining a 2-fold symmetry. Fourteen independent models were built. We calcu-lated the NSD between each pair of models, without realignment, to analyze their discrepancy and to select the most typical model (number 0), i.e., the model with lowest deviation from the others. The reconstruction converged toward a structure (Figure 4) with a distinc-tive pear shape for the two GyrA-CTDs, on both sides of GyrA59 and with a large interaction surface. The added density for each CTD began at the carboxyl-end of GyrA59 (green residues in Figure 4), which was not a modeling constraint. Surprisingly, the main part of the CTD lay in the lower part of the full protein, with the convention of the active site facing upward (yellow resi-dues in Figure 4A). This position is unexpected because
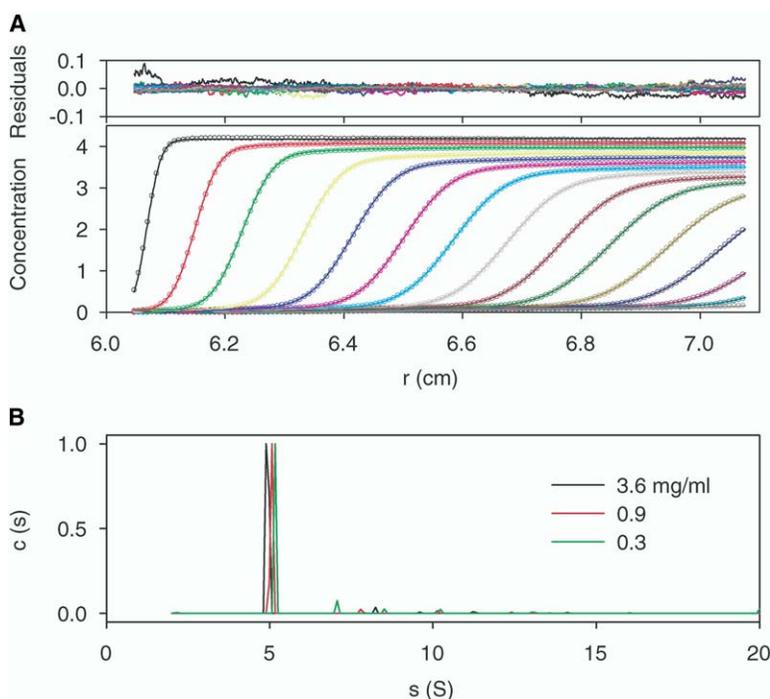
Figure 1. Analytical Ultracentrifugation of GyrA

(A) Modeling of the sedimentation velocity profiles of GyrA at 0.9 mg/ml. The symbols represent the experimental profiles as a function of time and distance from the axis of rotation, after the start of the sedimentation at 42,000 rpm and 6°C. The curves represent the theoretical fits, and the residuals are their differences with the corresponding experimental profiles. Concentrations are in units of fringe displacement in the interference optical system. For clarity, only every second profile and every ten experimental points used in the analysis are shown.
(B) Sedimentation coefficient distributions $c(s)$ calculated for GyrA. The distributions are normalized to the main peak values, at 6°C.

previous work conjectured the GyrA-CTD to be above the active-site level (Corbett et al., 2004; Kampranis et al., 1999), based on an electron-microscopy model (Kirchhausen et al., 1985). The fourteen independent models are ranked in Table 1 by increasing NSD value over all residues, with the most typical model (number 0) as reference. They fell into three categories. First, the consensus models were the seven models with NSD values below one for the entire structure, and below 1.7 for only one GyrA-CTD, indicating a very good agreement between their shapes. Figure 5A shows only one CTD of a typical consensus model. Note that overall NSD values were lower than those over one CTD, because they include the GyrA59 structure, which was common to all Credo models. Second, three models (number 1, 11, and 3) were considered as outliers with overall NSD values above 1.5, corresponding to NSD values above 2.4 over only one GyrA-CTD. Their added densities for GyrA-CTD were indeed different from the consensus: either more elongated (model 1, Figure 5C), or entirely at the top (model 3) or at the bottom (model 11) of GyrA59. Third, the remaining four models (number 4, 5, 6, and 13) had very high NSD values: above 3 and 7, over all the residues, and over one CTD, respectively.
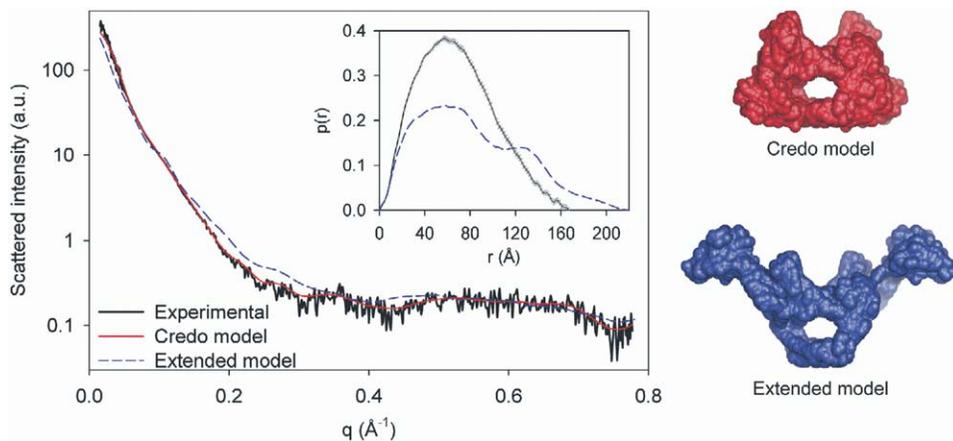

Figure 2. Small-Angle X-Ray Scattering of GyrA in Solution

Experimental data (black line) are shown as a function of the momentum transfer $q = 4\pi \sin\theta/\lambda$, in comparison to a typical model reconstructed by Credo (red line) and with the extended model (blue dashed line, see Discussion). The pair distribution function $p(r)$ of GyrA calculated from the SAXS data is shown in the inset. The curve represents the distribution of interatomic distances within GyrA: the molecule has a maximal length of 167 Å in solution.
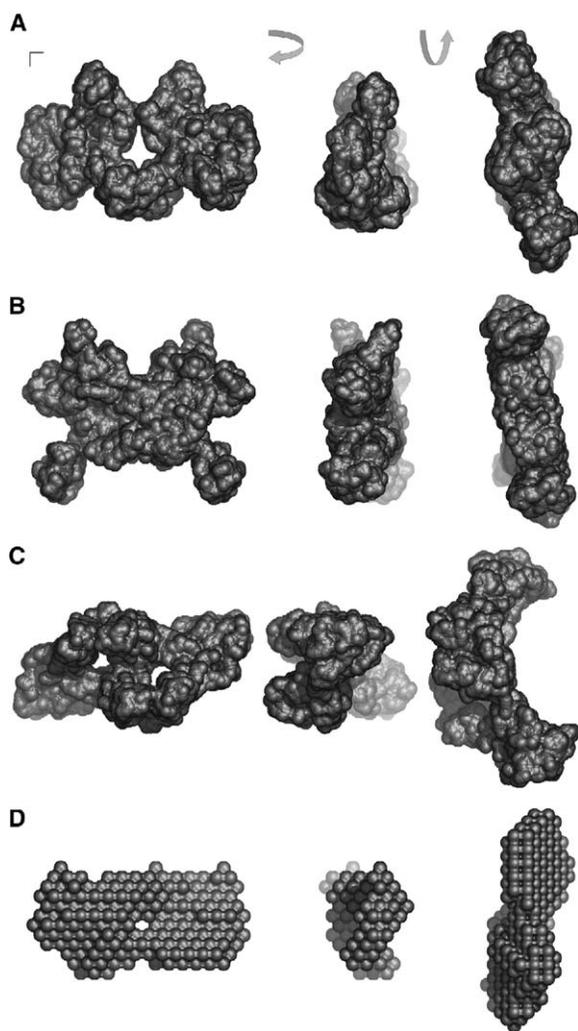
Figure 3. GyrA Models Obtained with Gasbor

(A–C) Typical models.
(D) Average model representing the common structural features of 20 independent models. The surfaces were built from a sphere radius of 5 Å for each residue. The views are respectively from front, side, and bottom; the length of the axes is 10 Å.

However, they shared a similar CTD shape shown in Figure 5B for one of them. Their CTD densities did not begin at the carboxyl-end of GyrA59 and hence would not correspond to an alternative conformation within GyrA in solution. Surprisingly, they showed CTD densities similar to the consensus, but mirrored in the main GyrA transversal plane. As scattering is a function of interatomic distances within the proteins and not of orientation, it does not distinguish between enantiomorph mates, i.e. mirror images, nor do the modeling programs. We hence mirrored these four models and realigned them with the reference model of GyrA (Figure 5B). The resulting NSD values over one CTD (in brackets in Table 1) were about 1.9, indicating a good similarity with the reference model. All these values remained lower than those of the three outliers. The corresponding overall NSD values were much less informative as they include the enantiomorph mate of

GyrA59, which is physically impossible. During the simulated annealing, Credo might have selected an enantiomorph state for the free dummy residues (and not for the fixed ones), yielding these four models. Rather than outliers, we considered them as "pseudo-enantiomorphs," and hence supporting the consensus structure.

Discussion

Ab Initio Modeling
During the ab initio reconstruction of the GyrA structure, we applied two constraints. First, GyrA was assumed to be a dimer in solution and a 2-fold symmetry constrained both Gasbor and Credo searches. Cross-linking experiments indicated GyrA to be a dimer (Klevan and Wang, 1980). Our analytical ultracentrifugation experiments show that unmodified GyrA sediments in solution as a single species, a dimer. As the GyrA59 carboxyl ends are at the far edges of the molecule, the 2-fold symmetry of its crystal structure is quite likely to be preserved within the full-length GyrA. Second, GyrA59 was assumed to conserve its crystallographic structure within the full-length GyrA in solution for the Credo searches. If the common structural features of the Gasbor models could suggest an intact GyrA59 structure in the middle of the GyrA density, the discrepancy of these models makes this support uncertain. However, cross-linking experiments on both GyrA59 dimer interfaces showed that GyrA59 remained dimeric in solution and that the locked gate mutants were able to bind and cleave DNA (Williams and Maxwell, 1999a, 1999b). These results support our second assumption.

The first attempt to reconstruct the global structure of GyrA with Gasbor failed to converge toward a consensus shape. As all the residues (874 per monomer) were free, it could result from too many possibilities of arranging them into the search volume. GyrA being an elongated protein also increases the search volume compared with a globular protein of the same mass. In contrast, with fewer degrees of freedom (only 352 free residues per monomer), the GyrA59 core being fixed to its crystallographic structure, Credo converged toward a unique structure.

GyrA Structure in Solution
Our velocity sedimentation results showed that GyrA is a dimer in solution. Ab initio modeling from small-angle X-ray scattering experiments on GyrA converged toward a unique structure: a dimeric GyrA59 core closely flanked by two additional pear-shaped densities in a low position with the convention of the active site facing upward (Figure 4A). The overall dimensions of this zigzag oblate ellipsoid are about 150 × 100 × 60 Å. When calculating their hydrodynamic properties at 6°C, the Credo models have on average an s value of 5.4 ± 0.1 S and an R_H of 54.0 ± 0.6 Å, in good agreement with the values obtained, independently, from analytical ultracentrifugation.

However, a different low-resolution structure was obtained from early electron microscopy: GyrA was found to be a dimer with a "V" shape of about 210 Å in width and 120 Å in height (Kirchhausen et al., 1985). This shape, much more extended than ours, was until now
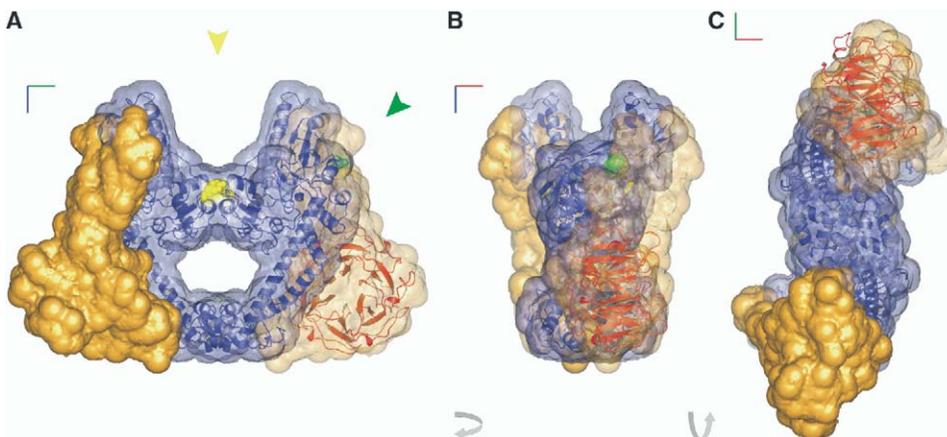
Figure 4. GyrA Solution Structure

The most typical model (model 0) obtained with Credo is represented as a surface with the fixed GyrA59 structure in blue (Morais Cabral et al., 1997), and, in orange, the added densities for GyrA-CTD on both sides. The active-site tyrosines are colored in yellow and the GyrA59 carboxyl in green, shown in space-fill and indicated by arrows in (A). The surface was built from a sphere radius of 5 Å for each residue. The GyrA59 crystallographic structure is shown in blue ribbons. The red ribbons represent the six-bladed "β pinwheel" domain of one GyrA-CTD, modeled from a homologous crystallographic structure (Corbett et al., 2004) and fitted into the density added by Credo. In this recto orientation, the blade numbers go from one to six, clockwise, starting from the top (for the front view A, as in Figure 7B). The views (A–C) are respectively from front, side, and bottom. The x axis is in red, y in green, and z in blue; their length is 10 Å.

assumed to be the conformation of GyrA, alone or within the gyrase holoenzyme. With a dimeric GyrA59 core, such an extended shape could be obtained with the two CTDs, not lying on its side as in our compact conformation, but apart, above the active-site level. We built such an extended model by rotating both CTDs from our compact model around the carboxyl-ends of GyrA59 (Figure 2) and we calculated its hydrodynamic and scattering properties. This extended conformation would yield an s value of 4.5 S and an R_H of 65 Å at 6°C, which differ by 15% from our analytical ultracentrifugation results. As Figure 2 shows, its scattered intensity and pair distribution function would also be clearly different from our experimental data. This extended conformation might be due to the sample preparation for the electron microscopy: the protein was dried onto a surface and platinum shadowed or stained. On the other hand, we performed our experiments in solution, with a solvent composition close to physiological, and found only compact conformations and none of our models showed such an extended conformation. Interestingly, this raises the possibility of a conformational change of GyrA, which we shall discuss later.

Position of GyrA-CTD within GyrA Structure

A high-resolution structure of GyrA-CTD from *E. coli* was built by homology modeling using the recent struc-ture from *B. burgdorferi* (Corbett et al., 2004). The two homologs share 27% identical and 49% similar amino acids, spread over the sequence of the crystallographic structure (*E. coli* residues 537–839, Figure 6). The hydrophobic patches are also mainly preserved through the sequences. The GyrA-CTD sequence from *E. coli* fits well to the 6-bladed β pinwheel fold, without any serious clashes (Figure 7B). Moreover, its surface shows a similar charge distribution (Figures 7C–7E): the β pinwheel faces are mainly negatively charged and almost all its rim is highly positively charged. For the *B. burgdorferi* structure, two thirds of this rim surface are also positively charged, but the remaining third, consisting of blades 2–3, is more negatively charged. However, two loops before strands C1 and C2, which were not seen in the crystallographic structure (Figure 6), are positively charged and could invert the charge distribution of the blade 2–3 surface.

In our solution structure built by Credo, two pear-shaped densities flank the dimeric GyrA59 core (Figure 4). Each one can account very well for a GyrA-CTD monomer. This rules out the possibility of our SAXS data being the result of multiple and coexisting conformations for GyrA. For such a mixture, the structure restored by the ab initio reconstruction would indeed be an average of these conformations. The added density would be distributed over the conformations and could not account for an intact GyrA-CTD. Given its shape,

Table 1. Normalized Spatial Discrepancy (NSD) between GyrA Models Built by Credo

	Consensus Models							Outlier Models			Pseudo-Enantiomorph Models[a]			
Models	0	12	9	10	8	2	7	1	11	3	13	6	5	4
NSD over all residues	Ref.	0.63	0.65	0.73	0.74	0.81	0.89	1.54	2.77	3.01	3.25 [1.86]	3.30 [1.92]	3.35 [1.85]	3.40 [1.88]
NSD over one CTD	Ref.	1.02	1.03	1.15	1.23	1.29	1.64	2.46	5.8	9.44	7.25 [1.87]	7.31 [1.96]	7.60 [1.88]	7.12 [1.98]

[a] Values in brackets were calculated for the enantiomorph mate realigned with the reference model of GyrA (number 0).
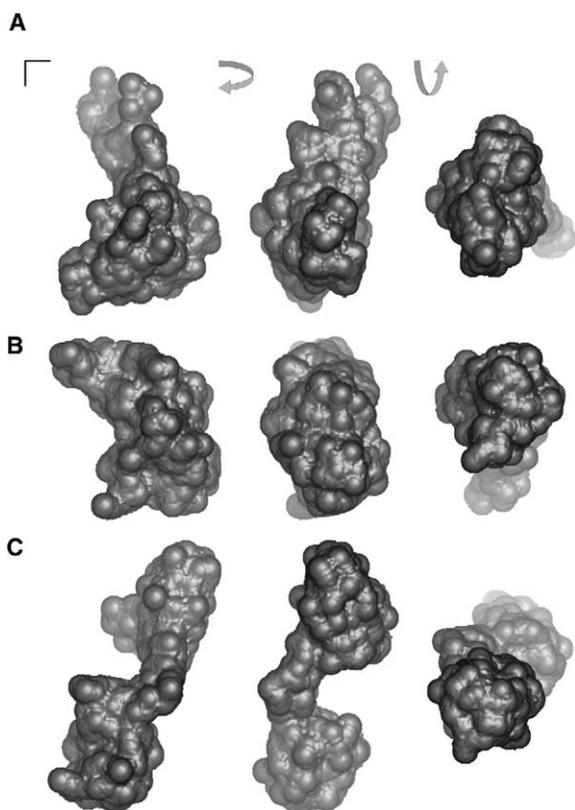
A

B

C

Figure 5. GyrA-CTD Models Obtained with Credo

(A) Example of a consensus model (number 0), (B) of a pseudo-enantiomorph models (number 13) realigned with the most typical model of GyrA (Figure 4), and (C) of an outlier model (number 1). For clarity, only one monomer of GyrA-CTD is shown. The surfaces were built from a sphere radius of 5 Å for each residue. The views are respectively from front, side, and bottom; the length of the axes is 10 Å.

only the lower and larger part of the density can accommodate the β pinwheel fold of the CTD, with its rim in contact with GyrA59 and its faces extending the main

zigzag plan of the protein (Figure 4C). The negative and positive character of the side surfaces of GyrA59 and CTD, respectively (Figure 7), corroborates this side-by-side orientation. The interaction between the two domains should be largely electrostatic. The tail of the pear-shaped density is large enough to account for the remaining residues, including the carboxyl-terminal residues that are not present in *B. burgdorferi*. It connects the GyrA59 carboxyl (green residues in Figure 4) to the β pinwheel and is long enough (about 30 Å) for the 14-amino-acid linker between them. Therefore, the first blade of the β pinwheel must be the uppermost one and only two orientations remain: a recto orientation (with blades 5–6 in contact with GyrA59, as in Figure 7B) or a verso orientation (with blades 2–3 contacting GyrA59). Because the two loops missing in the structure from *B. burgdorferi* could invert the charge of the blade 2–3 surface, from negative to positive, we cannot really rule out the verso orientation.

Insight into Supercoiling by DNA Gyrase

DNA gyrase catalyzes two main types of reaction. First, it can relax or decatenate DNA, but less efficiently than other type II topoisomerases. Second, it is the only topoisomerase able to actively introduce negative supercoils into DNA. If both types of reaction share the same core mechanism, the transport of a double-stranded DNA segment through a cleaved segment, they differ by the involvement of GyrA-CTD and by the minimal length of DNA bound to the enzyme. The deletion of GyrA-CTD turns gyrase into an enzyme unable to supercoil DNA, but more efficient for DNA relaxation and decatenation (Kampranis and Maxwell, 1996). The CTD hence inhibits the latter reactions. This truncated holoenzyme also binds a shorter length of DNA, about 30 base pairs (the G segment) around the cleavage site, like other type II topoisomerases, which cannot supercoil DNA and mainly rely on the DNA topology to present a T segment for capture (Lee et al., 1989; Peng and Marians, 1995). In our structure of the full-length GyrA (Figure 4), the CTDs are lying low on the GyrA59 sides, as far as possible from the cleavage active site.
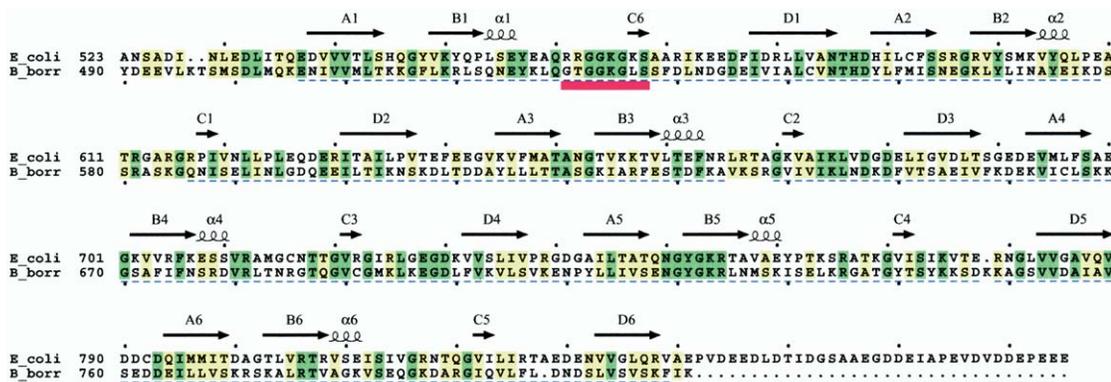

Figure 6. Alignment of GyrA-CTD Sequences from *E. coli* and *B. burgdorferi*

Identical residues are colored in green and similar ones in yellow. The secondary structural elements from the *B. burgdorferi* crystal structure are labeled A, B, C, and D for the strands and α for the helices followed by the number of the blade to which they belong. The residues present in the crystal structure are underlined in blue. The "GyrA box" is underlined in red.
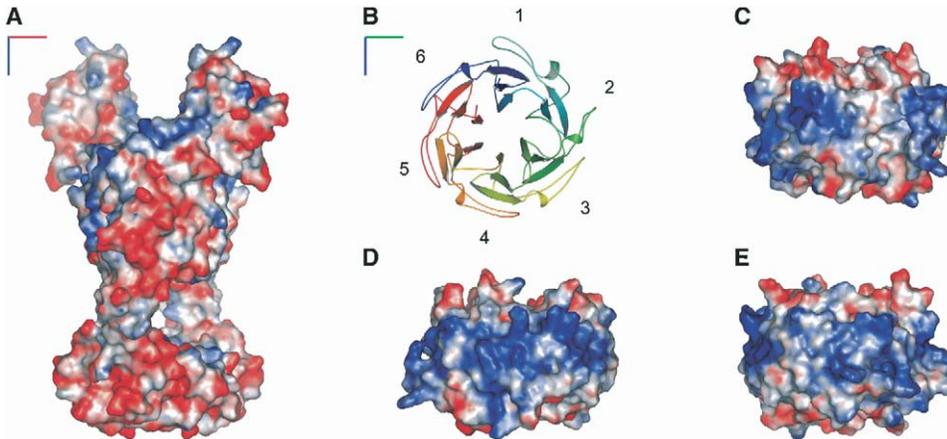
Figure 7. Electrostatic Surfaces of GyrA59 and GyrA-CTD β Pinwheel from *E. coli*

(A) Side view of the GyrA59 surface (Morais Cabral et al., 1997).

(B) Ribbon representation of GyrA-CTD β pinwheel built by homology modeling with the crystallographic structure from *B. burgdorferi* (Corbett et al., 2004). Blades one to six are colored from blue to red, clockwise (recto orientation, front view).

(C–E) Rim surface of GyrA-CTD β pinwheel with blades 1 and 2, 3 and 4, and 5 and 6 facing, respectively. Negatively charged surfaces are in red and positively charged surfaces in blue. The x axis is in red, y in green and z in blue; their length is 10 Å.

Such a compact conformation would minimize the obstruction of relaxation and decatenation by the CTDs and could be their actual conformation within GyrA during these reactions.

By contrast, the CTD is required for the supercoiling activity of DNA gyrase and actually confers this unique capacity to the enzyme (Kampranis and Maxwell, 1996). Figure 8 presents a schematic view of this reaction, commonly accepted for stages 2–4. The holoenzyme wraps ∼130 base pairs of DNA around itself in a right-handed manner (stage 2) (Liu and Wang, 1978; Orphanides and Maxwell, 1994). Because of this wrap, gyrase preferentially uses two segments of the same DNA molecule as the G and T segments. The central region of this DNA forms the G segment and should be bound around the cleavage active site by the positively charged surface, over about 30 base pairs, like other type II topoisomerases. FRET experiments have shown that GyrA-CTD from *B. burgdorferi* can bend DNA by about 180° over 40 base pairs (Corbett et al., 2004), presumably around its positive rim surface. However, we found that, without DNA, part of this surface interacts with GyrA59, so the CTDs have to move away to bind the DNA adjacent to the G segment. The initiation of the supercoiling reaction (stages 1–2 in Figure 8) would therefore be the binding of DNA probably near
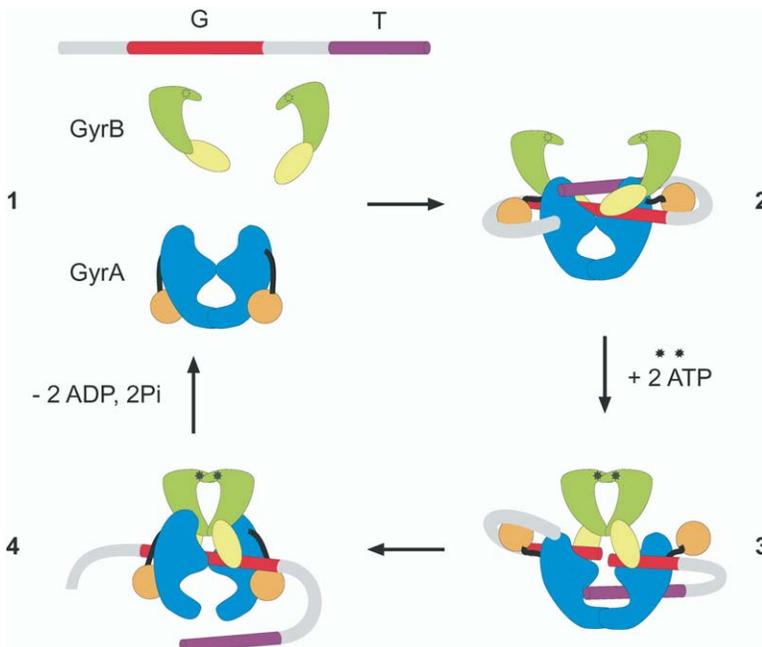

Figure 8. Schematic Views of Supercoiling by DNA Gyrase

The cleavage domain, GyrA59, is shown in blue, the wrapping domain, GyrA-CTD, in orange with the flexible linker in black, the ATPase domain of GyrB in green, and its carboxyl-terminal domain in yellow. The wrapping of the DNA around GyrA-CTDs should trigger their movement upward, in an extended conformation (stages 1 and 2). Gyrase transiently cleaves a DNA segment, the gate segment (G, in red), and transports another DNA segment (T, in purple) through this break before its religation (stages 3 and 4).

the cleavage active site in the first instance and then around the CTDs, forcing GyrA from a compact to an extended conformation. The "V" shape found by electron microscopy (Kirchhausen et al., 1985) could correspond to this extended conformation of GyrA. With a CTD above the active-site level (stage 2), a T segment could hence be presented above the G segment, forming a positive crossover that would be inverted by the holoenzyme (stage 3), creating two negative supercoils in the DNA (Brown and Cozzarelli, 1979). Since GyrA is a dimer, each CTD on each GyrA59 side can present a potential T segment, but the dimerization of GyrB upon ATP binding should select only one. This stage also causes the loss of the wrap, at least partially (Heddle et al., 2004).

If the GyrA-CTD confers on DNA gyrase its unique capacity to introduce negative supercoils, it is surprisingly preserved in most topo IVs that cannot supercoil DNA (Corbett et al., 2004; Ullsperger and Cozzarelli, 1996). Topo IV, another type II topoisomerase present in most bacteria, is a heterotetramer with its subunits, ParC and ParE, being close homologs of GyrA and GyrB, respectively. In some bacteria, ParC lacks the domain homologous to GyrA-CTD, but, in most bacteria, it has either a five- or a six-bladed CTD. The ParC-CTD from *E. coli*, which seems to contain only five blades, is also able to bend DNA, to nearly the same extent as GyrA-CTD from *B. burgdorferi*, but with a lower affinity (Corbett et al., 2004). Why does GyrA-CTD confer such a different capacity only to DNA gyrase? All ParC proteins lack an 8-amino-acid sequence highly conserved in all GyrA proteins and called the "GyrA box" (*E. coli* residues 561–568, Figure 6) (Ward and Newton, 1997). The recent crystallographic structure of the ParC-CTD from *Bacillus stearothermophilus* shows that missing the GyrA box breaks down the 6-bladed β pinwheel fold into an "open" β pinwheel. The breakage of the fold would explain why ParC-CTD is less efficient than GyrA-CTD in bending DNA (Hsieh et al., 2004). As both CTDs bend DNA to nearly the same extent (Corbett et al., 2004), the GyrA box should hence play a key role in wrapping DNA for supercoiling, in addition to its structural role, explaining the divergent activities of the two homologous enzymes. These residues are mainly basic and belong to the external loop that closes blade six of the β pinwheel (Figure 7B). We propose that it acts as an anchor into the DNA backbone. It would be more stabilizing at the end of the wrap rather than at its beginning. Because this loop closes blade six, it would corroborate the recto orientation of the β pinwheel, with blades 5-6 in contact with GyrA59. If the unique capacity of gyrase to introduce negative supercoils is due mainly to the GyrA box, this loop should be considered as a potential drug target.

In summary, experiments in solution allowed us to determine a low-resolution structure for the full-length A subunit of DNA gyrase. Analytical ultracentrifugation shows that GyrA is a dimeric and nonglobular protein. Ab initio modeling from small-angle X-ray scattering reveals the overall protein structure and the organization of its domains: a dimeric GyrA59 core closely flanked by two additional pear-shaped densities, in an unexpected low position. Each one accommodates very well a GyrA-CTD monomer built from a homologous

crystallographic structure. The low position of this wrapping domain strongly suggests a large conformation change of the enzyme upon DNA binding for supercoiling.

Experimental Procedures

Protein Purification
E. coli GyrA was overexpressed in pPH3-pLysS JM109 cells and purified as previously described (Maxwell and Howells, 1999). We further purified the protein through a gel filtration column (Superose 6 HR10/30 from Pharmacia) in 50 mM Tris-HCl (pH 7.5), 55 mM KCl, 5 mM DTT, and 5 mM MgCl$_2$, before concentration. GyrA concentration was determined spectrophotometrically using an extinction coefficient at 280 nm of 0.89 ml/mg/cm.

Analytical Ultracentrifugation
Sedimentation velocity experiments were performed at the Institut de Biologie Structurale in Grenoble, France, using a Beckman Optima XL-I analytical ultracentrifuge and an AN-60 TI rotor. Experiments were carried out at 6°C in 50 mM Tris-HCl (pH 7.5), 55 mM KCl, 5 mM DTT, and 5 mM MgCl$_2$. Two samples (420 μl) at protein concentrations of 0.3 and 0.9 mg/ml were loaded into 12 mm path cells and one sample (110 μl) at 3.6 mg/ml into a 3 mm path cell, and centrifuged at 42,000 rpm. We recorded interference optical scans, and absorbance scans in duplicates at 275 nm every 6 min using a 0.03 mm radial spacing.

We analyzed the sedimentation profiles with the software Sedfit, which takes advantage of a radial- and time-dependent noise subtraction, and directly models boundary profiles in terms of a continuous distribution of discrete and noninteracting species (Schuck, 2000). This allows the evaluation of the sedimentation coefficient (*s*). For each protein concentration, we modeled 30 experimental profiles with 200 generated sets of data for *s* values between 2 and 20 S on a radial grid of 500 points. We used a confidence level of 0.68 for the regularization procedure and checked the relevance of the results by Monte Carlo statistical analysis. The value of the hydrodynamic radius (R_H) was derived from the Svedberg equation: $s = M(1 - \rho\bar{v}) / (6\pi\eta R_H N_A)$, N_A being Avogadro's constant. We estimated the partial specific volume ($\bar{v}$) of GyrA from its amino acid composition to be 0.74 ml/g, the solvent density (ρ) to be 1.004 g/ml, and the solvent viscosity (η) to be 1.5 mPa·s, at 6°C using the software Sednterp (www.bbri.org/RASMB/rasmb.html).

Small-Angle X-Ray Scattering
We performed the SAXS experiments in solution at station 2.1 (Towns-Andrews et al., 1989) of the Synchrotron Radiation Source, Daresbury Laboratory, UK, following standard procedures. The protein solutions at 0.65 and 3.26 mg/ml were centrifuged for 5 min at 13,000 × g before being measured at 6°C. Scattering curves were collected with a two-dimensional multiwire proportional counter, at sample-to-detector distances of 1 and 4.25 min, at a wavelength (λ) of 1.54 Å, covering the momentum transfer range 0.008 < *q* < 0.78 Å^{-1} ($q = 4\pi\sin\theta /\lambda$, where 2θ is the scattering angle). To check for radiation damage and aggregation, the data were collected in 125 and 23 successive 1 min frames, respectively. The data were normalized to the intensity of the incident beam, radially integrated over a 60° sector, averaged over the frame number and divided out by the detector response. The scattering of the buffer was then subtracted and the low- and high-angle curves were merged over the *q* range of 0.05–0.15 Å using the software Primus (Konarev et al., 2003). The radius of gyration (R_g) was evaluated using the Guinier approximation: $I(q) = I(0)\exp(-q^2R_g^2/3)$ for $qR_g < 1.3$ (Guinier and Fournet, 1955), and also from the entire scattering curve with the indirect Fourier-transform program Gnom (Svergun, 1992). Gnom also provides the distance distribution function $p(r)$ of the particle and its maximum dimension D_{max}, defined as the point where $p(r)$ becomes zero. To determine $p(r)$, we left $p(0)$ and $p(D_{max})$ free, in the first instance, to judge whether the chosen *r* interval was correct. D_{max} was the lowest value yielding the lowest positive $p(D_{max})$, a stable $p(r)$ distribution upon D_{max} increase. $p(0)$ and $p(D_{max})$ were finally fixed to zero.

Ab Initio Modeling

Low-resolution models were generated by two ab initio programs Gasbor (version 1.8) and Credo (Petoukhov et al., 2002; Svergun et al., 2001). We set the search-volume diameter to D_{max} and D_{max} + 11 Å for Gasbor. All dummy residues (874 per monomer) were refined by Gasbor, and we fixed the GyrA59 residues to their C_α crystallographic position (PDB code 1ab4) and refined the remaining carboxyl-terminal residues (352 per monomer) by Credo. A 2-fold symmetry constrained both the Gasbor and Credo searches. Gasbor-independent models were superimposed and analyzed with the package Damaver (Volkov and Svergun, 2003) to construct the average model that represents the common structural features of all the reconstructions. The normalized spatial discrepancy (NSD) (Kozin and Svergun, 2001) between Credo-independent models was calculated, without realignment, with the program Distrms (M. Kozin, personal communication). For these low-resolution structures in solution, we calculated their sedimentation coefficient (s) and hydrodynamic radius (R_H) with the program Hydropro with a radius of 6 Å for the dummy residues (Garcia de la Torre et al., 2000). The scattered intensity and the pair distribution function of the extended model were calculated with Crysol (using the parameters determined for our Credo model) and Gnom, respectively (Svergun, 1992, 1995).

Homology Modeling

The GyrA-CTD sequences from *E. coli* (SP P09097) and from *B. burgdorferi* (SP O51396) were aligned using as a guide the published multiple sequence alignments (Corbett et al., 2004; Qi et al., 2002). The X-ray crystallographic structure of GyrA-CTD from *B. burgdorferi* (PDB code 1suu) was used as a template for homology modeling by the SWISS-MODEL server (optimize mode) (Guex and Peitsch, 1997; Schwede et al., 2003). The loop 607–617 was reconstructed and the geometry of the whole model optimized using the Discover module within InsightII (Accelrys), by a conjugate gradient algorithm and consistent valence force field.

Structural figures were made with PyMol (www.pymol.org), electrostatic surfaces calculated with APBS (Baker et al., 2001) and mapped to the protein surface using M.G. Lerner's script (www-personal.umich.edu/~mlerner/Pymol/). The alignment figure was generated by ESPript (Gouet et al., 1999).

References

Baker, N.A., Sept, D., Joseph, S., Holst, M.J., and McCammon, J.A. (2001). Electrostatics of nanosystems: application to microtubules and the ribosome. Proc. Natl. Acad. Sci. USA *98*, 10037–10041.

Berger, J.M., Gamblin, S.J., Harrison, S.C., and Wang, J.C. (1996). Structure and mechanism of DNA topoisomerase II. Nature *379*, 225–232.

Brown, P.O., and Cozzarelli, N.R. (1979). A sign inversion mechanism for enzymatic supercoiling of DNA. Science *206*, 1081–1083.

Champoux, J.J. (2001). DNA topoisomerases: structure, function, and mechanism. Annu. Rev. Biochem. *70*, 369–413.

Corbett, K.D., Shultzaberger, R.K., and Berger, J.M. (2004). The C-terminal domain of DNA gyrase A adopts a DNA-bending β-pinwheel fold. Proc. Natl. Acad. Sci. USA *101*, 7293–7298.

Drlica, K., and Malik, M. (2003). Fluoroquinolones: action and resistance. Curr. Top. Med. Chem. *3*, 249–282.

Emmerson, A.M., and Jones, A.M. (2003). The quinolones: decades of development and use. J. Antimicrob. Chemother. *51* (Suppl. 1), 13–20.

Fass, D., Bogden, C.E., and Berger, J.M. (1999). Quaternary changes in topoisomerase II may direct orthogonal movement of two DNA strands. Nat. Struct. Biol. *6*, 322–326.

Garcia de la Torre, J., Huertas, M.L., and Carrasco, B. (2000). Calculation of hydrodynamic properties of globular proteins from their atomic-level structure. Biophys. J. *78*, 719–730.

Gouet, P., Courcelle, E., Stuart, D.I., and Metoz, F. (1999). ESPript: analysis of multiple sequence alignments in PostScript. Bioinformatics *15*, 305–308.

Guex, N., and Peitsch, M.C. (1997). SWISS-MODEL and the Swiss-PdbViewer: an environment for comparative protein modeling. Electrophoresis *18*, 2714–2723.

Guinier, A., and Fournet, G. (1955). Small-Angle Scattering of X-Rays (New York: Wiley Press).

Hande, K.R. (1998). Clinical applications of anticancer drugs targeted to topoisomerase II. Biochim. Biophys. Acta *1400*, 173–184.

Heddle, J.G., Mitelheiser, S., Maxwell, A., and Thomson, N.H. (2004). Nucleotide binding to DNA gyrase causes loss of DNA wrap. J. Mol. Biol. *337*, 597–610.

Hsieh, T.J., Farh, L., Huang, W.M., and Chan, N.L. (2004). Structure of the topoisomerase IV C-terminal domain: A broken beta-propeller implies a role as geometry facilitator in catalysis. J. Biol. Chem. *279*, 55587–55593.

Kampranis, S.C., and Maxwell, A. (1996). Conversion of DNA gyrase into a conventional type II topoisomerase. Proc. Natl. Acad. Sci. USA *93*, 14416–14421.

Kampranis, S.C., Bates, A.D., and Maxwell, A. (1999). A model for the mechanism of strand passage by DNA gyrase. Proc. Natl. Acad. Sci. USA *96*, 8414–8419.

Kirchhausen, T., Wang, J.C., and Harrison, S.C. (1985). DNA gyrase and its complexes with DNA: direct observation by electron microscopy. Cell *41*, 933–943.

Klevan, L., and Wang, J.C. (1980). Deoxyribonucleic acid gyrase-deoxyribonucleic acid complex containing 140 base pairs of deoxyribonucleic acid and an alpha 2 beta 2 protein core. Biochemistry *19*, 5229–5234.

Konarev, P.V., Volkov, V.V., Sokolova, A.V., Koch, M.H.J., and Svergun, D.I. (2003). PRIMUS: a Windows PC-based system for small-angle scattering data analysis. J. Appl. Crystallogr. *36*, 1277–1282.

Kozin, M.B., and Svergun, D.I. (2001). Automated matching of high- and low-resolution structural models. J. Appl. Crystallogr. *34*, 33–41.

Lee, M.P., Sander, M., and Hsieh, T. (1989). Nuclease protection by Drosophila DNA topoisomerase II. Enzyme/DNA contacts at the strong topoisomerase II cleavage sites. J. Biol. Chem. *264*, 21779–21787.

Lewis, R.J., Singh, O.M., Smith, C.V., Skarzynski, T., Maxwell, A., Wonacott, A.J., and Wigley, D.B. (1996). The nature of inhibition of DNA gyrase by the coumarins and the cyclothialidines revealed by X-ray crystallography. EMBO J. *15*, 1412–1420.

Liu, L.F., and Wang, J.C. (1978). Micrococcus luteus DNA gyrase: active components and a model for its supercoiling of DNA. Proc. Natl. Acad. Sci. USA *75*, 2098–2102.

Maxwell, A., and Howells, A.J. (1999). Overexpression and purification of bacterial DNA gyrase. In DNA Topoisomerase Protocols, Part I: DNA Topology and Enzymes, N. Osheroff and M.-A. Bjornsti, eds. (Totowa, New Jersey: Humana Press), pp. 135–144.

Maxwell, A., and Lawson, D.M. (2003). The ATP-binding site of type II topoisomerases as a target for antibacterial drugs. Curr. Top. Med. Chem. *3*, 283–303.

Morais Cabral, J.H., Jackson, A.P., Smith, C.V., Shikotra, N., Maxwell, A., and Liddington, R.C. (1997). Crystal structure of the breakage-reunion domain of DNA gyrase. Nature *388*, 903–906.

Orphanides, G., and Maxwell, A. (1994). Evidence for a conformational change in the DNA gyrase-DNA complex from hydroxyl radical footprinting. Nucleic Acids Res. *22*, 1567–1575.

Peng, H., and Marians, K.J. (1995). The interaction of Escherichia coli topoisomerase IV with DNA. J. Biol. Chem. *270*, 25286–25290.

Petoukhov, M.V., Eady, N.A., Brown, K.A., and Svergun, D.I. (2002). Addition of missing loops and domains to protein models by x-ray solution scattering. Biophys. J. *83*, 3113–3125.

Pommier, Y., Pourquier, P., Fan, Y., and Strumberg, D. (1998). Mechanism of action of eukaryotic DNA topoisomerase I and drugs targeted to the enzyme. Biochim. Biophys. Acta *1400*, 83–105.

Qi, Y., Pei, J., and Grishin, N.V. (2002). C-terminal domain of gyrase A is predicted to have a β-propeller structure. Proteins *47*, 258–264.

Reece, R.J., and Maxwell, A. (1991). The C-terminal domain of the Escherichia coli DNA gyrase A subunit is a DNA-binding protein. Nucleic Acids Res. *19*, 1399–1405.

Schuck, P. (2000). Size-distribution analysis of macromolecules by sedimentation velocity ultracentrifugation and Lamm equation modeling. Biophys. J. *78*, 1606–1619.

Schwede, T., Kopp, J., Guex, N., and Peitsch, M.C. (2003). SWISS-MODEL: an automated protein homology-modeling server. Nucleic Acids Res. *31*, 3381–3385.

Svergun, D.I. (1992). Determination of the regularization parameter in indirect-transform methods using perceptual criteria. J. Appl. Crystallogr. *25*, 495–503.

Svergun, D.I., Barberato, C., and Koch, M.H.J. (1995). CRYSOL—a program to evaluate X-ray solution scattering of biological macromolecules from atomic coordinates. J. Appl. Crystallogr. *28*, 768–773.

Svergun, D.I., Petoukhov, M.V., and Koch, M.H. (2001). Determination of domain structure of proteins from X-ray solution scattering. Biophys. J. *80*, 2946–2953.

Towns-Andrews, E., Berry, A., Bordas, J., Mant, G.R., Murray, P.K., Roberts, K., Sumner, I., Worgan, J.S., Lewis, R., and Gabriel, A. (1989). Time-resolved X-ray-diffraction station—X-ray optics, detectors, and data acquisition. Rev. Sci. Instrum. *60*, 2346–2349.

Ullsperger, C., and Cozzarelli, N.R. (1996). Contrasting enzymatic activities of topoisomerase IV and DNA gyrase from Escherichia coli. J. Biol. Chem. *271*, 31549–31555.

Volkov, V.V., and Svergun, D.I. (2003). Uniqueness of ab initio shape determination in small-angle scattering. J. Appl. Crystallogr. *36*, 860–864.

Wall, M.K., Mitchenall, L.A., and Maxwell, A. (2004). Arabidopsis thaliana DNA gyrase is targeted to chloroplasts and mitochondria. Proc. Natl. Acad. Sci. USA *101*, 7821–7826.

Wang, J.C. (2002). Cellular roles of DNA topoisomerases: a molecular perspective. Nat. Rev. Mol. Cell Biol. *3*, 430–440.

Ward, D., and Newton, A. (1997). Requirement of topoisomerase IV parC and parE genes for cell cycle progression and developmental regulation in Caulobacter crescentus. Mol. Microbiol. *26*, 897–910.

Wigley, D.B., Davies, G.J., Dodson, E.J., Maxwell, A., and Dodson, G. (1991). Crystal structure of an N-terminal fragment of the DNA gyrase B protein. Nature *351*, 624–629.

Williams, N.L., and Maxwell, A. (1999a). Locking the DNA gate of DNA gyrase: investigating the effects on DNA cleavage and ATP hydrolysis. Biochemistry *38*, 14157–14164.

Williams, N.L., and Maxwell, A. (1999b). Probing the two-gate mechanism of DNA gyrase using cysteine cross-linking. Biochemistry *38*, 13502–13511.